

# Luminescence studies of dysprosium doped strontium aluminate white light emitting phosphor by combustion route

Ishwar Prasad Sahu<sup>1</sup> · D. P. Bisen<sup>1</sup> · Nameeta Brahme<sup>1</sup> ·  
Raunak Kumar Tamrakar<sup>2</sup> · Ravi Shrivastava<sup>3</sup>

Received: 10 May 2015 / Accepted: 30 July 2015 / Published online: 5 August 2015  
© Springer Science+Business Media New York 2015

**Abstract** In the present investigation dysprosium doped strontium aluminate phosphor was prepared by combustion synthesis method. The crystal structure of the prepared phosphor was consistent with standard monoclinic phase with a space group  $P2_1$ . According to the TEM analysis, the particle size was found to be in the nanometer range. The trap parameters which are mainly activation energy (E), frequency factor (s) and order of the kinetics (b) were evaluated by using the peak shape method. Under the ultraviolet (365 nm) excitation, photoluminescence (PL) spectra showed characteristic emission bands at 480 (blue), 573 (yellow) and 670 nm (red) due to  ${}^4F_{9/2} \rightarrow {}^6H_{15/2}$ ,  ${}^4F_{9/2} \rightarrow {}^6H_{13/2}$  and  ${}^4F_{9/2} \rightarrow {}^6H_{11/2}$  transitions of  $Dy^{3+}$  ions. Combination of these three emissions constituted as white light confirmed by the Commission Internationale de L'Eclairage (CIE) chromatic coordinate diagram and possible mechanism of white light emitting  $SrAl_2O_4:Dy^{3+}$  phosphor was also investigated. The value of correlated color temperature (CCT) was found, well within the defined acceptable range (5965 K). The mechanoluminescence (ML) intensity of  $SrAl_2O_4:Dy^{3+}$  phosphor increases linearly with increasing impact velocity of the moving piston. Thus, the present investigation indicates the piezoelectricity was responsible to produce ML in prepared phosphor.

## 1 Introduction

In the field of light sources, for more than 25 years, the argon mercury discharge fluorescent lamp has been widely used for general lighting purpose. As far as the environmental issues are concerned, the requirement for mercury free fluorescent lamps for general lighting has become a fundamental subject for light source manufacturers and hence also for researchers [1]. Many attempts have been made to develop mercury free light sources. The demand has quickly increased and has become more and more important in order to avoid the use of hazardous ingredients and environmentally unsafe materials. Lamp industries aim to reduce the quantity of mercury from fluorescent lamps and develop alternative mercury free excitation sources such as plasma devices [2, 3].

In recent years, light emitting diode (LED) devices for general lighting purposes are of increasing interest. Hence, solid state lighting (SSL) has become an interesting field for researchers especially with respect to white light sources. SSL is an energy efficient lighting technology, which offers advantages such as low power consumption, long lifetime, and environmental friendliness. It is estimated that even if only 50 % SSL were to be achieved and displaced current white lighting technologies, the electricity used for lighting would be cut by 62 % [4, 5]. However, commercial white light emitting diodes (WLEDs) produced by combining a blue LED chip with yellow emitting phosphor cannot meet the requirement of general illumination due to their poor color rendering index (<50) and unsatisfactory high color temperature (<3500 K) because of weak red emission [6, 7]. Thus, it is necessary to search phosphors that can be efficiently excited in the UV range, to enhance the luminous efficiency. There is a growing interest in rare-earth ion activated aluminates metal oxide

✉ Ishwar Prasad Sahu  
ishwarprasad1986@gmail.com

<sup>1</sup> School of Studies in Physics and Astrophysics, Pt. Ravishankar Shukla University, Raipur, C.G., India

<sup>2</sup> Department of Applied Physics, Bhilai Institute of Technology, Durg, C.G., India

<sup>3</sup> Department of Physics, ICFAI University, Raipur, C.G., India

phosphors because of their interesting optical properties, which make them a part of almost every display device [8].

Strontium aluminates are the most widely used members of the alkaline earth aluminates  $\text{MAl}_2\text{O}_4$  ( $\text{M} = \text{Ca}, \text{Sr}, \text{and Ba}$ ). Among those various phosphors,  $\text{SrAl}_2\text{O}_4$  has attracted much interest in recent years owing to its excellent luminescent properties such as long duration and high brightness [9]. In addition,  $\text{SrAl}_2\text{O}_4$  material is chemically more stable than sulfide phosphors. Rare-earth doped  $\text{SrAl}_2\text{O}_4$  materials present interesting luminescence properties and attractive optical characteristics. As one of the most promising phosphors,  $\text{Eu}^{2+}$  doped  $\text{SrAl}_2\text{O}_4$  shows strong luminescence and especially long persistent luminescence in green region [10].

Rare earth  $\text{Dy}^{3+}$  ions have two dominant emission bands in the blue region (460–480 nm) due to  ${}^4\text{F}_{9/2} \rightarrow {}^6\text{H}_{15/2}$  transition and in the yellow region (550–580 nm) due to  ${}^4\text{F}_{9/2} \rightarrow {}^6\text{H}_{13/2}$  transition [11, 12]. It is possible to achieve near white light emission by adjusting the yellow to blue intensity ratio value. Consequently,  $\text{Dy}^{3+}$  activated luminescent materials have attracted much attention, because of their significant applications as potential single phase white phosphors [13].

With the development of scientific technologies on materials, several chemical synthesis techniques, such as co-precipitation, sol–gel, microwave, and combustion synthesis methods have been applied to prepare the rare earth ions activation alkaline earth aluminate and/or its phosphors. All of these methods were conducted in liquid phases so that each component can be accurately controlled and uniformly mixed. The solid-state reaction process has been used intensively for phosphor synthesis, but this process often results in poor homogeneity and requires high calcinating temperature. Furthermore, the grain size of phosphor powders prepared through solid state reaction method is in several tens of micrometers. Phosphors of small particles must be obtained by grinding the larger phosphor particles. These processes easily introduce additional defects and greatly reduce luminescence efficiency [14, 15]. The combustion process to prepare the precursor powders, however, is very easy and only takes a few minutes, being extensively applied to the preparation of various oxide materials. This synthesis technique makes use of the heat energy liberated by the redox exothermic reaction at a relative low igniting temperature between metal nitrates and urea or other fuels. Furthermore, the process is also safe, instantaneous and energy saving [16, 17].

The present paper reports dysprosium doped strontium aluminates phosphor prepared by combustion synthesis techniques. Their structural characterizations were investigated by X-ray diffraction (XRD), transmission electron microscopy (TEM), field emission scanning electron microscope (FESEM) coupled with energy dispersive

X-ray spectroscopy (EDS) and Fourier transform infrared spectroscopy (FTIR). The luminescent properties were investigated on the basis of thermoluminescence (TL), TL emission spectra, photoluminescence (PL), lifetime measurement and mechanoluminescence (ML) in detail.

## 2 Experimental

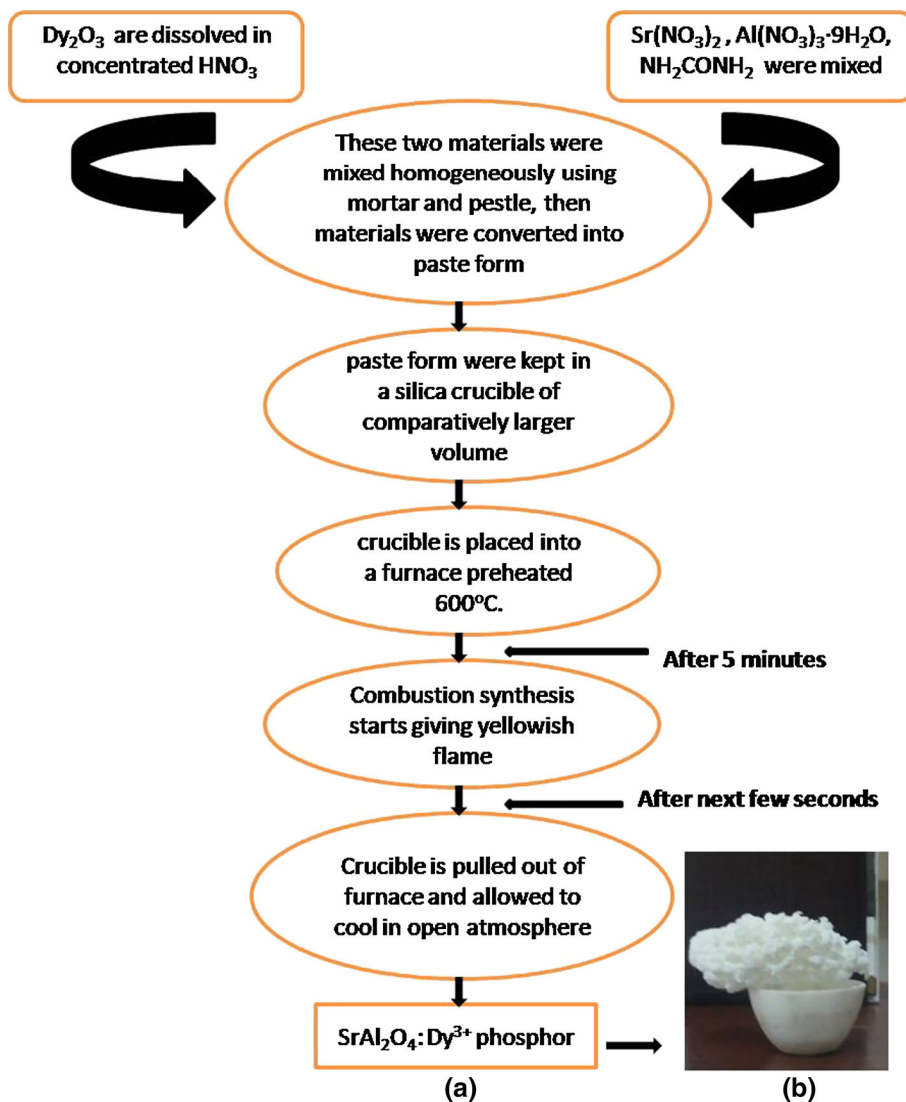
### 2.1 Phosphor synthesis

Dysprosium doped strontium aluminate namely  $\text{SrAl}_2\text{O}_4:\text{Dy}^{3+}$  phosphor was prepared by the combustion synthesis method starting with the strontium nitrate [ $\text{Sr}(\text{NO}_3)_2$  (99.90 %)], aluminum nitrate [ $\text{Al}(\text{NO}_3)_3 \cdot 9\text{H}_2\text{O}$  (99.90 %)], urea [ $\text{NH}_2\text{CONH}_2$  (99.99 %)] and small amount of boric acid [ $\text{H}_3\text{BO}_3$  (99.90 %)] was used as the flux while the urea was used as fuel. For preparing  $\text{SrAl}_2\text{O}_4:\text{Dy}^{3+}$  phosphor, powders were weighted according to the stoichiometric amounts. Strontium nitrate [ $\text{Sr}(\text{NO}_3)_2$  (99.90 %)], aluminum nitrate [ $\text{Al}(\text{NO}_3)_3 \cdot 9\text{H}_2\text{O}$  (99.90 %)] and urea [ $\text{NH}_2\text{CONH}_2$  (99.99 %)] were dissolved into enough deionized water to obtain transparent solution. In addition to it, dysprosium oxide [ $\text{Dy}_2\text{O}_3$  (99.99 %)] taken as activators was dissolved in concentrated nitric acid ( $\text{HNO}_3$ ; 99.90 %) with slight heating and stirred for 2 h at 70 °C, before being transferred to silica crucible. A crucible was used as a container within which chemical reaction took place. After the solution was transferred into the crucible with comparatively larger volume, it was placed into a furnace already maintained at temperature of 600 °C. Initially, the dehydration by boiling the solution was started, followed by evolving decomposition under the presence of large amounts of gases (oxides of carbon, nitrogen, and ammonia). Then the reagent was spontaneously ignited and underwent combustion to produce foamy and voluminous ash. The mixture froths and swells forming foam, which ruptures with a flame and glows to incandescence. This continues for next few seconds and as it is over, crucible was taken out of the furnace and kept in open to allow cool in open atmosphere. Upon cooling, we get the fluffy form of material, which was crushed using agate pestle and mortar to get material in the powder form [18]. The whole process took not more than 5 min (Fig. 1).

### 2.2 Characterization techniques

The crystal structure of the prepared  $\text{SrAl}_2\text{O}_4:\text{Dy}^{3+}$  phosphor was characterized by powder XRD analysis. Powder XRD pattern was obtained from Bruker D8 advanced X-ray powder diffractometer using  $\text{CuK}\alpha$  radiation and the data were collected over the  $2\theta$  range 15°–65°. The crystal structure of the prepared  $\text{SrAl}_2\text{O}_4:\text{Dy}^{3+}$  phosphor was

**Fig. 1 a, b** Schematic diagram for the synthesis of  $\text{SrAl}_2\text{O}_4:\text{Dy}^{3+}$  phosphor via combustion synthesis method



verified with the help of Joint Committee of Powder Diffraction Standard Data (JCPDS) file (JCPDS: 34-0379). Particle size of prepared phosphor was determined by TEM using TECHNAI G2 by FEI. The phosphor required for TEM analysis was prepared by dispersing the  $\text{SrAl}_2\text{O}_4:\text{Dy}^{3+}$  phosphor in methanol using an ultrasound bath technique. A drop of this dispersed suspension was put onto 200-mesh carbon coated copper grid and then dried in open atmosphere. The morphological images of prepared  $\text{SrAl}_2\text{O}_4:\text{Dy}^{3+}$  phosphors were collected by the FESEM. The samples were coated with a thin layer of gold (Au) and then the surface morphology of the prepared phosphor was observed by a FESEM; ZEISS Ulta Plus-55 operated at the acceleration voltage of 10 kV. An EDS spectrum was used for the elemental (qualitative and quantitative) analysis of the sintered phosphor. FTIR spectra were recorded in the middle infrared region ( $4000\text{--}400\text{ cm}^{-1}$ ) with the help of IR Prestige-21 by SHIMADZU. For investigating the

functional groups ( $4000\text{--}1400\text{ cm}^{-1}$ ) and finger print region ( $1400\text{--}400\text{ cm}^{-1}$ ) of IR spectra, potassium bromide was mixed with prepared  $\text{SrAl}_2\text{O}_4:\text{Dy}^{3+}$  phosphor. TL glow curves were recorded with the help of TLD reader 1009I by Nucleonix (Hyderabad, India Pvt. Ltd.) and TL emission spectrum was recorded with the help of different band pass interference ( $400\text{--}700\text{ nm}$ ) filter. The excitation and emission spectra were measured by a spectrofluorophotometer (SHIMADZU, RF-5301 PC) using the Xenon lamp as excitation source. The decay curves were obtained using a Perkin Elmer fluorescent spectrometer with the proper excitation under a UV lamp ( $365\text{ nm}$ ). The ML measurement was observed by the home made lab system comprising a RCA-931A photomultiplier tube (PMT). The ML glow curve can be plotted with the help of SM-340 application software installed in a computer attached with the storage oscilloscope. All measurements were carried out at the room temperature.

### 3 Results and discussion

#### 3.1 XRD analysis

XRD patterns of the  $\text{SrAl}_2\text{O}_4:\text{Dy}^{3+}$  phosphors are shown in Fig. 2. The prepared sample gives broader and intense peaks, indicating smaller grain size and lower crystallinity degrees.  $\text{SrAl}_2\text{O}_4$  has two phases, a high temperature hexagonal phase ( $\beta$ -phase) and a low temperature monoclinic phase ( $\alpha$ -phase). The obtained XRD pattern confirms the existence of a predominant monoclinic  $\text{SrAl}_2\text{O}_4$  phase which is estimated to be around 89 %. This was determined through relative intensity ratio match technique using the ICDD PDF 96-200-2285 and JCPDS file No. 34-0379 files, which indicates the crystal structure of the prepared powders is in the low-temperature monoclinic phase with a space group  $\text{P}2_1$ . No peak other than those from the parent is resolved in the XRD pattern, which suggests the formation of single phase material. The five dominant peaks in the XRD patterns are located at 19.96, 28.46, 29.27, 29.98, and 35.11°, these principle peaks were identified as the (0 1 1), ( $\bar{2}$  1 1), (2 2 0), (2 1 1) and (0 3 1) planes that characterize the crystal line  $\text{SrAl}_2\text{O}_4$  structure.

It is to be noted that the small amount of doped rare earth ions have almost no effect on the basic crystal structure.  $\text{SrAl}_2\text{O}_4$  undergoes a phase transition from monoclinic to hexagonal at 800 °C temperature. The synthesis temperature at 600 °C is lower than that used

normally in sol–gel and solid-state reaction methods, and this temperature most fraction of particle are in monoclinic phase. The other impurity phases such as  $\beta$ - $\text{SrAl}_2\text{O}_4$ ,  $\text{Sr}_3\text{Al}_2\text{O}_6$  and  $\text{Sr}_4\text{Al}_{14}\text{O}_{25}$  were not observed [16].

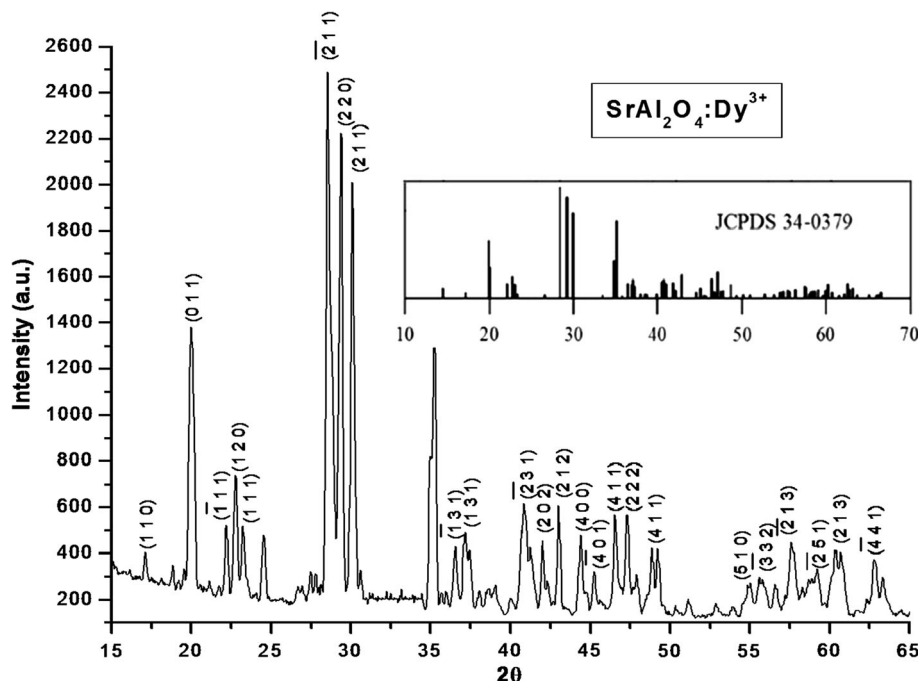
#### 3.2 Transmission electron microscopy (TEM)

Figure 3 displays a typical TEM image of the prepared dysprosium doped strontium aluminate phosphor under combustion at 600 °C for 5 min. The phosphor powders are irregular spherical particles, the surfaces of the foams show a lot of cracks, voids and pores formed by the escaping gases during combustion reaction. It reveals that the mean size is about ~30–50 nm. Compared with the phosphor prepared via the traditional solid state reaction method, the grain size is much larger but has good crystallinity. It is ascribed that solid state reaction requires a high calcining temperature, which induces sintering and aggregation of particles, and it is an advantage for perfect crystal formation.

#### 3.3 Field emission scanning electron microscopy (FESEM)

In order to determine the surface morphology, grain size, and shape of the synthesized phosphor, typical FESEM measurements are carried out and are presented in Fig. 4. This typical structure was observed earlier in  $\text{SrAl}_2\text{O}_4$ :

**Fig. 2** XRD patterns of  $\text{SrAl}_2\text{O}_4:\text{Dy}^{3+}$  phosphor





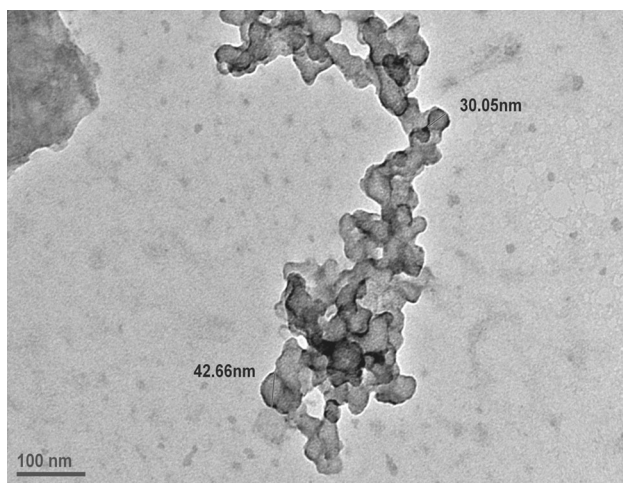


**Fig. 3** TEM images of  $\text{SrAl}_2\text{O}_4:\text{Dy}^{3+}$  phosphor

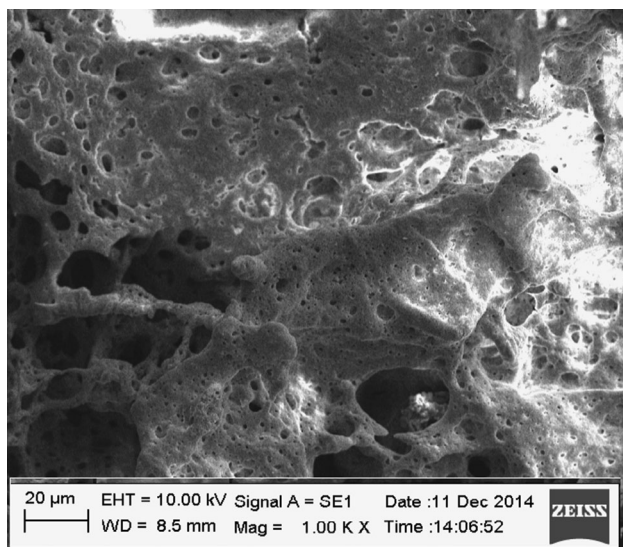


**Fig. 4** FESEM image of  $\text{SrAl}_2\text{O}_4:\text{Dy}^{3+}$  phosphor

$\text{Eu}^{2+}$ ;  $\text{SrAl}_2\text{O}_4:\text{Eu}^{2+}$ ,  $\text{Dy}^{3+}$  phosphors and it is probably due to the escaping gases during combustion reaction. In dysprosium doped strontium aluminate samples the crystallites are seen to be uniformly distributed and the voids are occupied. The reason for lots of vacant space may be that the mixture containing stoichiometric amount of redox mixture when heated rapidly at  $600\text{ }^\circ\text{C}$  boils and undergoes dehydration followed by decomposition generating combustible gases ( $\text{NO}_2$ ) [19]. The volatile combustible gases ignite and burn with a flame and then provide conditions for formation of phosphor lattice with dopants. The large amount of escaping or dissipates gases prevents the material from sintering and then provides conditions for formation of nano-crystalline phase. Also, as the gases escape they leave voluminous, foaming and crystalline fine powder occupying the entire volume of the firing container and

have no chance of forming agglomeration unlike in other conventional processes.

The surface of the powders samples show lots of voids and pores formed by the escaping gases during the combustion process. When a gas is escaping under high pressure, pores are formed with the formation of small particles near the pores, and this is clearly illustrated by Fig. 4. The microstructure of these samples reflects the inherent nature of the combustion process. The non uniform and irregular shapes of the particles as shown can be attributed to the non-uniform distribution of temperature and mass flow in the combustion flame.

### 3.4 Energy dispersive X-ray spectroscopy (EDS)

The chemical composition (qualitative and quantitative) of the  $\text{SrAl}_2\text{O}_4:\text{Dy}^{3+}$  phosphor was measured using EDS spectrum. Figure 5 shows the EDS spectra of  $\text{SrAl}_2\text{O}_4:\text{Dy}^{3+}$  phosphor. EDS is a standard procedure for identifying and quantifying elemental composition of sample area as small as a few nanometers. The existence of dysprosium (Dy) in the phosphors is clear in their corresponding EDS spectra. They revealed no other emissions apart from strontium (Sr), aluminum (Al), oxygen (O) and dysprosium (Dy) in  $\text{SrAl}_2\text{O}_4:\text{Dy}^{3+}$  in the EDX spectrum. All the expected elements with their relative ratios are presented in Table 1, and intense peaks of EDS spectra confirm the presence of elements in of  $\text{SrAl}_2\text{O}_4:\text{Dy}^{3+}$  phosphor. The EDS analysis of the chemical composition of the phosphor confirms this experimental evidence.

### 3.5 Fourier transform infrared (FTIR) spectroscopy

FTIR spectroscopy is a quick and precise measurement technique for qualitative species measurement. The FTIR analysis is an important tool in facilitating a better understanding of the properties of the material obtained. Spectroscopically, the middle infrared ( $4000\text{--}400\text{ cm}^{-1}$ ) region is extremely useful for the study of organic and inorganic

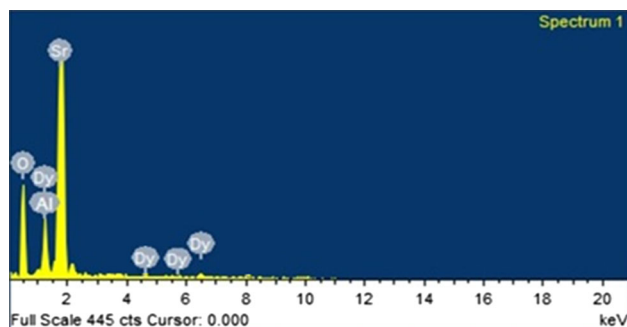


**Fig. 5** EDS spectra of  $\text{SrAl}_2\text{O}_4:\text{Dy}^{3+}$  phosphor

**Table 1** Chemical composition of SrAl<sub>2</sub>O<sub>4</sub>:Dy<sup>3+</sup> phosphor

Sr. No.	Standard	Elements	Atomic (%)	Weight (%)
1	Al <sub>2</sub> O <sub>3</sub>	O K	54.03	78.25
2	Al <sub>2</sub> O <sub>3</sub>	Al K	14.48	13.65
3	SrF <sub>2</sub>	Sr L	28.95	7.71
4	DyF <sub>3</sub>	Dy L	2.54	0.39
Total			100	100

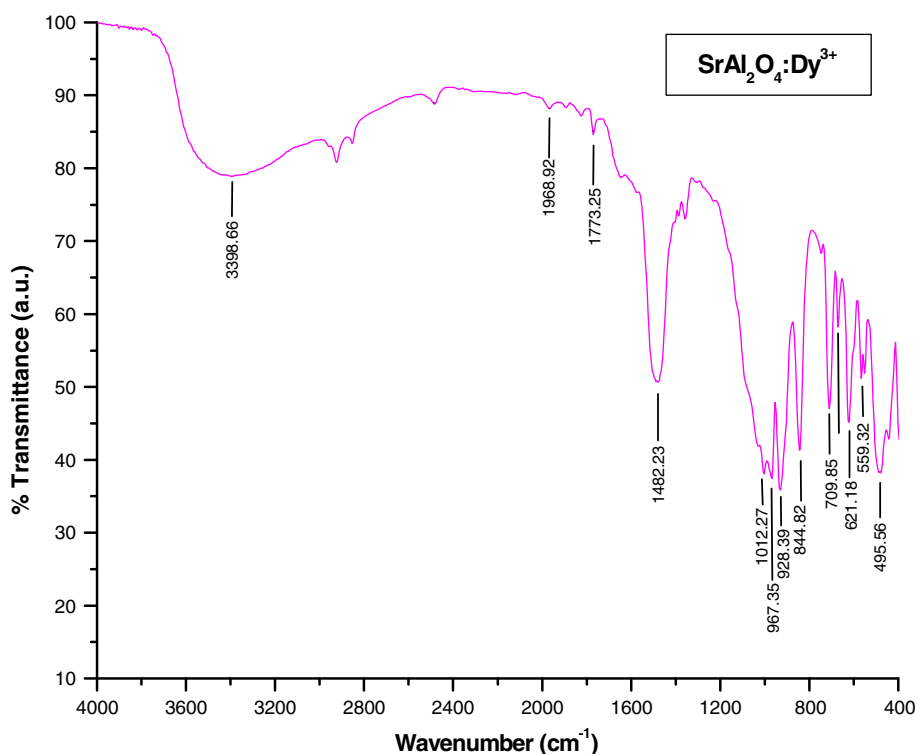
compounds. The FTIR transmittance spectrum of the SrAl<sub>2</sub>O<sub>4</sub>:Dy<sup>3+</sup> phosphors obtained is shown in Fig. 6. The IR spectrum of SrAl<sub>2</sub>O<sub>4</sub>:Dy<sup>3+</sup> phosphor contains clearly exhibited bands in the region [strong band ~3398.66 cm<sup>-1</sup> and around ~1900–1600 cm<sup>-1</sup> (weak shoulders)] of hydroxyl group showing the stretching and bending vibration of O–H groups. The hydroxyl group in sintered phosphor might be due to presence of moisture through environment. In the IR spectra of phosphor shows the strong peak at ~1482.23 cm<sup>-1</sup>. The exact origin of this peak, however, is not very clear. The bands located at ~1482.23 cm<sup>-1</sup>, could not be assigned to the metal nitrate formed as intermediates during synthesis process [20].

According to the crystal structure of SrAl<sub>2</sub>O<sub>4</sub>, the coordination number of strontium can be 8 and 6. Therefore, Sr<sup>2+</sup> can occupy two alternative lattice sites, the eight

coordinated Sr<sup>2+</sup> site [SrO<sub>8</sub> (Sr<sub>1</sub> site)] and the six coordinated Sr<sup>2+</sup> site [SrO<sub>6</sub> (Sr<sub>2</sub> site)], and one other independent cation sites, namely Al<sup>3+</sup> [AlO<sub>4</sub>] also exists in the crystal lattice. Al<sup>3+</sup> cations occupy the tetrahedral sites. Dy<sup>3+</sup> ions can occupy four alternative lattice sites and the coordination number of dysprosium can be 6, 7, 8 and 9 (Dy<sub>1</sub>, Dy<sub>2</sub>, Dy<sub>3</sub> and Dy<sub>4</sub> respectively). It's hard for Dy<sup>3+</sup> ions to incorporate the tetrahedral [AlO<sub>4</sub>] symmetry but they can easily incorporate octahedral [SrO<sub>8</sub>] or cubic [SrO<sub>6</sub>]. Another fact that supports that the radius of Dy<sup>3+</sup> (0.99 Å) is very close to that of Sr<sup>2+</sup> (about 1.12 Å) rather than Al<sup>3+</sup> (0.57 Å). Therefore, the Dy<sup>3+</sup> ions are expected to occupy the Sr<sup>2+</sup> sites in the SrAl<sub>2</sub>O<sub>4</sub>:Dy<sup>3+</sup> phosphor [21, 22].

In the presented spectrum the transmittance bands of aluminates groups were clearly evident in finger print region (1400–400 cm<sup>-1</sup>). In the finger print region several sharp bands are typical metal oxygen absorptions O–Al–O, Sr–O, Al–O stretching frequencies were found. The bands around ~1000–400 cm<sup>-1</sup> are typically assigned to the IR active vibration modes of SrAl<sub>2</sub>O<sub>4</sub>. The symmetric bonding of O–Al–O appeared at 844.82, 495.56 cm<sup>-1</sup>. The anti-symmetric stretching bands between 709.85, 621.18, 559.32 cm<sup>-1</sup> are attributed to the Sr–O vibrations. The symmetric stretching of Al–O appeared at 1012.27, 967.35, 928.39, 1012.27, 967.35, and 928.39 cm<sup>-1</sup> [23].

**Fig. 6** FTIR Spectra of SrAl<sub>2</sub>O<sub>4</sub>:Dy<sup>3+</sup> phosphor



### 3.6 Thermoluminescence (PL)

Thermoluminescence (TL) or more specifically Thermally Stimulated Luminescence (TSL) is stimulated thermally after initial irradiation given to a phosphor by some other means ( $\alpha$ -rays,  $\beta$ -rays,  $\gamma$ -rays, UV-rays and X-rays). Thermally stimulated luminescence (TSL) is the phenomenon of emission of light from a solid which has been previously exposed to ionizing radiation under conditions of increasing temperature. The band theory of solid is normally used to explain this phenomenon [24, 25]. When a solid is irradiated, electrons and holes are produced. The defects in the solids results in the presence of localized energy level within the forbidden gap. On irradiation, electron and holes can be trapped at these sites. When the solid is heated, these trapped electrons/holes get enough thermal energy to escape from the trap to the conduction band (or valence band). From here they may get trapped again or may recombine with trapped holes/electrons. The site of recombination is called recombination center. If this recombination is radiative, then the center is called luminescence center. Alternatively a trapped hole can be released by heating which can recombine with a trapped electron resulting in luminescence [26].

TL is a good way to detect the combination emission caused by thermal de-trapping of carriers. The energy corresponding to the glow peak is equal to the trap depth. What has to be emphasized is that traps and carriers (electrons and holes) may be produced by irradiation, but they are also created during sample processing. In order to understand the characteristics of the trapping centers in TL, TL profiles of glow curves were examined with plotting TL intensity against temperature for the  $\text{SrAl}_2\text{O}_4:\text{Dy}^{3+}$  phosphor. The photo induced electrons are released thermally and recombined with the holes. The TL properties were measured to estimate the phosphorescence characteristic of the  $\text{SrAl}_2\text{O}_4:\text{Dy}^{3+}$  phosphor [27].

The TL measurements were carried out as follows. First, the sample of approximately (8 mg) is weighted and irradiate at different times (10, 20, 30 min) using 365 nm UV source. Then, TL was observed while the sample was heated up to 300 °C at a constant heating rate of 5 °C/s. In the TL study, the mass of the sample was fixed (8 mg), and every time took the fresh sample for observation. Figure 7 shows the TL glow curve of  $\text{SrAl}_2\text{O}_4:\text{Dy}^{3+}$  phosphor. The TL glow peak occurred arising at 94.15 °C which arise due to defects (created by UV irradiation and during the synthesis process) and these peak positions remained constant with UV irradiation time. From the TL glow curve, it is seen that, initially TL intensity increase with increasing UV irra-

diation time. TL intensity was maximum for 20 min of UV exposure, after that they started to decrease. It is predicted that with the increasing UV irradiation time, greater number of charge carriers are released which increases the trap density results in increased TL intensity (density of charge carrier may have been increasing), but after a specific exposure (20 min) traps start to destroy results in decrease in TL intensity. The decreasing of charge carriers density may be a reason for the low TL intensity at higher irradiation time (30 min irradiation time) [28]. The luminescence process may be explained as follows:

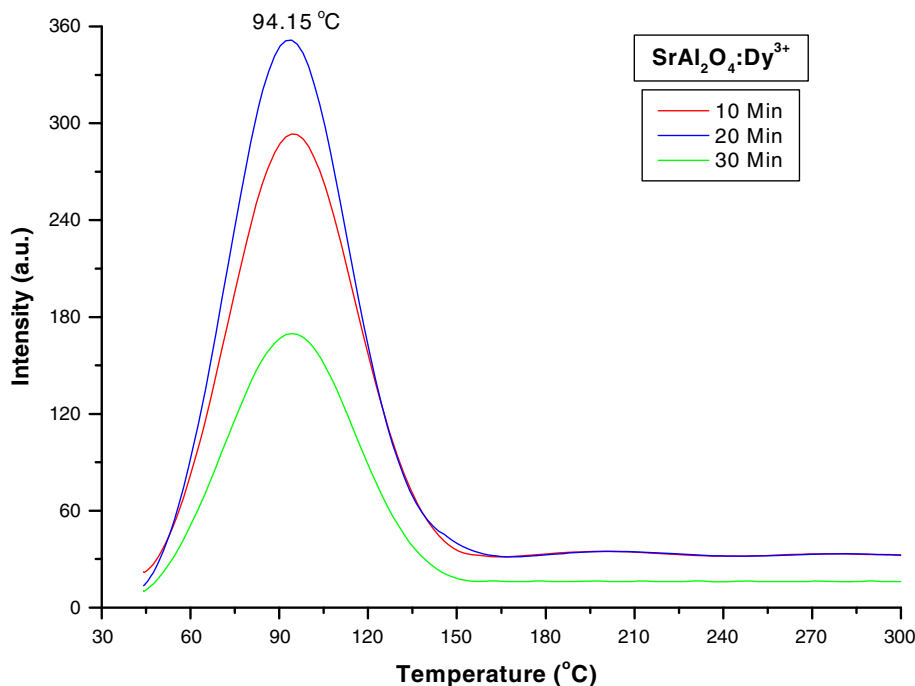
When trivalent metallic ions, such as  $\text{Dy}^{3+}$  are incorporated into a host lattice and substitute divalent metallic ions, the charge balancing is necessarily required. Due to these chemically nonequivalent substitutions, an excess of positive charge in the host lattice must be compensated. One possible way of charge compensation mechanism is that two  $\text{Dy}^{3+}$  ions replace three  $\text{Sr}^{2+}$  ions to balance the charge of these phosphors, which create two  $\text{Dy}'_{\text{Sr}}$  positive defects and one  $\text{V}''_{\text{Sr}}$  negative defect.



For  $\text{SrAl}_2\text{O}_4:\text{Dy}^{3+}$  the incorporation of alkali metal ions can neutralize the charge generated by  $\text{Dy}^{3+}$  substitution for  $\text{Sr}^{2+}$ , and thus stabilize the structure and enhance the luminescence.  $\text{Dy}^{3+}$  ions have been often used as co-dopants in the previously developed aluminate and silicate based materials. When divalent alkaline earth ions, such as  $\text{Sr}^{2+}$ ,  $\text{Ca}^{2+}$ ,  $\text{Ba}^{2+}$ , are substituted by trivalent  $\text{Dy}^{3+}$  in the alkaline earth silicates and aluminates, various defects can be induced due to the charge compensation mechanism. Furthermore the oxygen vacancies are also present. All these vacancies present make up trap levels [29].

In  $\text{SrAl}_2\text{O}_4$ , the most probable centers which can be observed are the V centers (a hole trapped at a cation vacancy) and F centers (an electron trapped at an anion vacancy). When the sample is irradiated with UV radiation most of the excitation energy associated with the excited carriers (electrons or holes) will be transferred via the host directly to the luminescence centers of  $\text{Dy}^{3+}$  followed by characteristic emission of  $\text{Dy}^{3+}$  immediately. However part of the excitation energy will be stored when electrons and holes are trapped in the trap levels. When the phosphor is heated, the thermal energy excites the filled traps to release carriers and is transferred via the host to the  $\text{Dy}^{3+}$  followed by the recombination of electrons and holes in the luminescence centers and give rise to luminescence. In the practical system the electron traps and the hole traps may not be both equally important in terms of their contribution to the light emission [30].

**Fig. 7** TL glow curve of SrAl<sub>2</sub>O<sub>4</sub>:Dy<sup>3+</sup> phosphor



### 3.7 Determination of kinetic parameters

The trapping centers or defects in a material play a major role in the luminescence process. TL measurements are obtained after turning off the irradiating source and monitoring the thermally stimulated luminescence under a condition of gradually increasing temperature. The shape and position of the resultant TL glow curve can be analyzed to obtain information on the various parameters of the trapping process [31, 32].

The determination of trapping parameters is of importance to find the material’s suitability for various applications. Whenever a trapped charge carrier (electron or hole) is considered to be released by thermal activation (as in TL) the usual mathematical approach is to consider the probability of finding these in a particular potential energy arrangement with a Maxwellian statistical distribution of energies at various temperatures. If a trap is considered as a potential well, then E is called trap depth and as the temperature is increased, the probability of finding the trapped carriers with this energy E (so that they can escape) increases exponentially by:  $e^{-E/kT}$ , where k is Boltzmann constant [33]. Semi-classically, assuming phonon interaction the problem of thermal activation of trapped charge carriers can be worked out to give the probability rate of escape as:

$$\tau^{-1} = P = s e^{-E/kT} \tag{2}$$

The factor “s” has the dimension of s<sup>-1</sup> and is hence called the frequency factor. In many phosphors, this factor is only

slowly varying with temperature and can be considered a constant for a particular trap. If one considers the trap as a potential well then value “s” represents the product of the number of times an electron hits the well (in an attempt to escape from the well) and the wall reflection coefficient.

The TL parameters i.e. activation energy (E), frequency factor (s) and shape factor ( $\mu_g$ ), for the prominent glow peaks of prepared phosphor were calculated using the peak shape method [34] are shown in Table 2. The relationship between the frequency factor ‘s’ and the activation energy ‘E’ is given by the Eq. (3)

$$\frac{\beta E}{kT_m^2} = s \left[ 1 + (b - 1) \frac{2kT_m}{E} \right] \exp(E/KT_m) \tag{3}$$

where, k is Boltzmann constant, b is order of kinetics, T<sub>m</sub> is temperature of peak position, and β is the heating rate. In the present work β = 5 °C/s. Trap depth for second order kinetics is calculated using the Eq. (4)

$$E = 2kT_m \left( 1.76 \frac{T_m}{\omega} - 1 \right) \tag{4}$$

where, ω is the total half width intensity ω = τ + δ, τ is the half width at the low temperature side of the peak (τ = T<sub>m</sub> - T<sub>1</sub>); δ is the half width towards the fall-off side of the glow peak (δ = T<sub>2</sub> - T<sub>m</sub>), and T<sub>m</sub> is the peak temperature at the maximum. The shape factor  $\mu_g = \delta/\omega$ . The shape factor ( $\mu_g$ ) is to differentiate between first and second order TL glow peak. ( $\mu_g$ ) = 0.39–0.42 for the first order kinetics, ( $\mu_g$ ) = 0.42–0.48 for the mixed order kinetics and ( $\mu_g$ ) = 0.49–0.52 for the second order kinetics [35].



**Table 2** Shape factor ( $\mu_g$ ), activation energy (E) and frequency factor ( $s^{-1}$ ) for UV irradiated  $\text{SrAl}_2\text{O}_4:\text{Dy}^{3+}$  phosphor

UV min	HTR	$T_1$ (°C)	$T_m$ (°C)	$T_2$ (°C)	$\tau$ (°C)	$\delta$ (°C)	$\omega$ (°C)	$\mu_g = \delta/\omega$	Activation energy	Frequency factor
10	5	67.25	94.15	121.23	26.90	27.08	53.98	0.50	0.70	$1.34 \times 10^9$
20	5	68.86	94.15	118.63	25.29	24.48	49.77	0.49	0.75	$1.11 \times 10^{10}$
30	5	68.86	94.15	120.54	25.29	26.39	51.68	0.51	0.73	$4.10 \times 10^9$

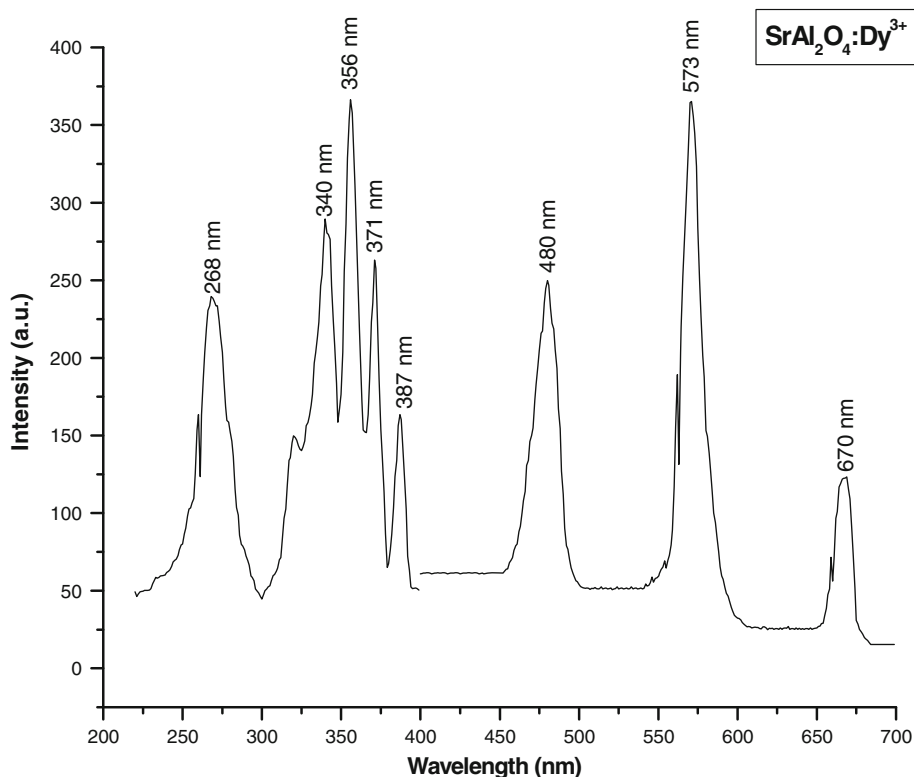
The effect of different UV exposures on the  $\text{SrAl}_2\text{O}_4:\text{Dy}^{3+}$  phosphor and different TL parameters like trap depth shape factor, frequency factor is calculated (Table 2). In our case, value of shape factor ( $\mu_g$ ) is lies between 0.49 and 0.51, which indicates that it is a case of non-first order kinetics, approaching towards second order kinetics.

### 3.8 Photoluminescence (PL)

In order to study the luminescence properties of the prepared  $\text{SrAl}_2\text{O}_4:\text{Dy}^{3+}$  phosphor, the excitation and emission spectra were recorded and shown in Fig. 8. The excitation spectra were observed in the range of 200–400 nm and emission spectra were recorded in the range of 400–700 nm. In Fig. 8, the excitation spectrum of  $\text{Dy}^{3+}$  doped  $\text{SrAl}_2\text{O}_4$ , the peaks which range from 200 to 400 nm are due to 4f–4f transitions of  $\text{Dy}^{3+}$ , while the broad band excitation peaking at 268 nm can be attributed to the

charge transfer state (CTS) of  $\text{Dy}^{3+} \rightarrow \text{O}^{2-}$ . Since this phosphor can efficiently emit yellow composition under the 300–400 nm excitation range, it is feasible to suggest that this phosphor has a potential application in white LEDs. The excitation spectrum of  $\text{SrAl}_2\text{O}_4:\text{Dy}^{3+}$  shows strong excited peak at 356 nm and less intense at 340, 371 and 387 nm which are ascribed to the transitions from the ground state to excitation states in the  $4f^9$  configuration of  $\text{Dy}^{3+}$  but not easy to be clearly assigned due to the dense and somewhat overlapped levels of 4f configuration of  $\text{Dy}^{3+}$  in the high energy region. When the  $\text{SrAl}_2\text{O}_4:\text{Dy}^{3+}$  phosphor was excited at 356 nm, simultaneous emissions of blue (480 nm), yellow (573 nm) and red (670) nm position were observed. Notice that the red emission is less intense than the blue and yellow emissions. These three different emission bands originated from the one origin owing to their having the same excitation wavelength. The transitions involved in blue, yellow and red bands of  $\text{Dy}^{3+}$

**Fig. 8** Excitation and emission spectra of  $\text{SrAl}_2\text{O}_4:\text{Dy}^{3+}$  phosphor



ion are well known and have been identified as  ${}^4F_{9/2} \rightarrow {}^6H_{15/2}$ ,  ${}^4F_{9/2} \rightarrow {}^6H_{13/2}$  and  ${}^4F_{9/2} \rightarrow {}^6H_{11/2}$  transitions respectively. One can also find that the emission lines of  $Dy^{3+}$  are broadened somewhat because there are several Stark levels for the  ${}^4F_{9/2} \rightarrow {}^6H_J$  levels [36].

It is well known that the former weak blue emission at 480 nm ( ${}^4F_{9/2} \rightarrow {}^6H_{15/2}$ ) is corresponded to the magnetic dipole transition, which hardly varies with the crystal field strength around  $Dy^{3+}$  ions. While the later, stronger yellow emission at 573 nm ( ${}^4F_{9/2} \rightarrow {}^6H_{13/2}$ ) belongs to the hypersensitive forced electric dipole transition, which is strongly influenced by the outside surrounding environment. According to the Judd–Ofelt theory [37], when  $Dy^{3+}$  locates at a low symmetry local site without inversion symmetry, a yellow emission according to the electric dipole transition ( ${}^4F_{9/2} \rightarrow {}^6H_{13/2}$ ) will be dominant. Conversely, a magnetic dipole transition ( ${}^4F_{9/2} \rightarrow {}^6H_{15/2}$ ) will predominate in the emission spectra, resulting in a strong blue emission. In our case, the yellow emission ( ${}^4F_{9/2} \rightarrow {}^6H_{13/2}$ ) will dominate. The strong yellow emission is also beneficial to generate white light emission. Moreover, the hardly perceptible transition ( ${}^4F_{9/2} \rightarrow {}^6H_{13/2}$ ) emission at 573 nm can be observed, which is also due to the disordered crystal field and is corresponding to the structural study. It is notice that the red emission is less intense than the blue and yellow emissions. It is well known that the ( ${}^4F_{9/2} \rightarrow {}^6H_{13/2}$ ) transition is hypersensitive and therefore, its intensity strongly depends on the host, while the ( ${}^4F_{9/2} \rightarrow {}^6H_{15/2}$ ) transition is less sensitive to the host. The optical properties of the material are often influenced by the structure of the matrix and synthesis technique [38].

However, in  $Dy^{3+}$  singly doped samples, which are in our current interest,  $Dy^{3+}$  is not only the supplier of traps but also an activator itself. A process of emitting the white light in  $SrAl_2O_4:Dy^{3+}$  phosphor is illustrated schematically

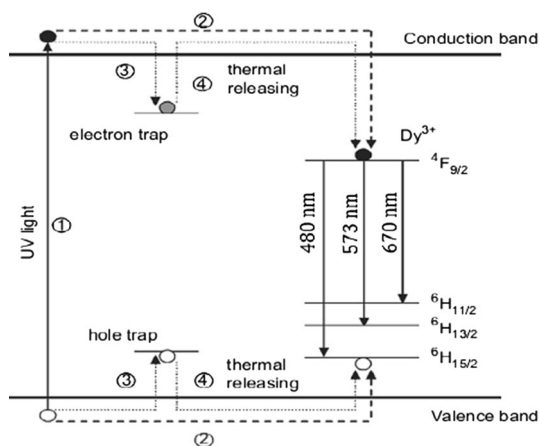


**Fig. 9** Schematic diagram of the mechanism in  $SrAl_2O_4:Dy^{3+}$  phosphor

in Fig. 9. After irradiation with the ultraviolet light (process numbered [1]), most of the excitation energy associated with the excited carriers (electrons or holes) will be transferred via the host directly to the luminescence centres,  $Dy^{3+}$ , followed by the  $Dy^{3+}$  4f emissions as the immediate luminescence (process [2]). However, part of the excitation energy will be stored when some of the excited carriers drop into the traps (process [3]), instead of returning to the ground states. Later, with thermal excitation at proper temperature, these carriers will be released from the traps and transferred via the host to the  $Dy^{3+}$  ions, followed by the characteristic  $Dy^{3+}$  emissions as long afterglow (process [4]). In the practical system, the electron traps and the hole traps may not be both equally abundant or important in terms of their contribution to the white light emission, as suggested in Fig. 9 [39, 40].

### 3.9 CIE chromaticity coordinate

In general, color coordinates are one of the important factors for evaluating phosphors color. The luminescence color of the samples excited under 356 nm has been characterized by the CIE (Commission International de l’Eclairage) 1931 chromaticity diagram. The emission spectrum of the  $SrAl_2O_4:Dy^{3+}$  phosphor was converted to the CIE 1931 chromaticity using the photoluminescent data and the interactive CIE software (CIE coordinate calculator) diagram as shown in Fig. 10.

Every natural color can be identified by (x, y) coordinates that are disposed inside the ‘chromatic shoe’ representing the saturated colors. Luminescence colors of  $SrAl_2O_4:Dy^{3+}$  phosphor are placed in ( $x = 0.320$ ,

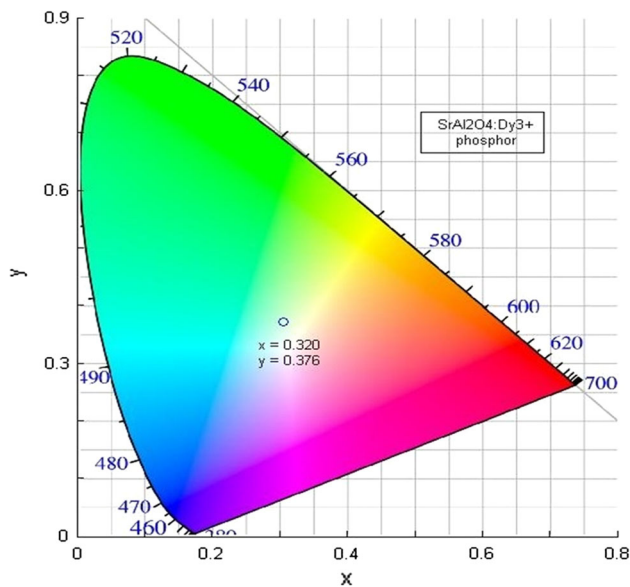


**Fig. 10** CIE chromaticity diagram of  $SrAl_2O_4:Dy^{3+}$  phosphor

$y = 0.376$ ), which is represented by the circle symbol ["o"]. It indicates that the color coordinates of  $\text{SrAl}_2\text{O}_4\text{:Dy}^{3+}$  phosphor are very close to the "ideal white light emission" ( $x = 0.333$ ,  $y = 0.333$ ) in chromaticity diagram. The chromatic co-ordinates of the luminescence of this phosphor are measure and reached to near white light emission [41].

### 3.10 Correlated color temperature (CCT)

Correlated color temperature (CCT) relates to the color of light produced by a light source, measured in degrees Kelvin. The CCT rating is an indication of how "warm" or "cool" the light source appears. The higher the CCT value, the cooler the lamp color will appear. The lower the number, the warmer the lamp color will appear. However, CCT is only one aspect of color. The color of light is measured using the scale, with the more orange color light being referred to as "warm white" and the whiter color light being referred to as "cool white". However, opposite to the temperature scale, lamps with a CCT rating below 3200 K are usually considered "warm" sources, while those with a CCT above 4000 K are usually considered "cool" in appearance. McCamy has proposed the analytical equation to calculate the CCT which is given [41] by

$$\text{CCT} = -449n^3 + 3525n^2 - 6823n + 5520.33 \quad (5)$$

where,  $n = (x - x_e)/(y - y_e)$  is the inverse slope line and ( $x_e = 0.332$ ,  $y_e = 0.186$ ) is the epicenter. Generally, the preferred CCT values range from 4000 to 6500 K but the range from 3500 to 7500 K may also be accepted. The calculated CCT Values of prepare  $\text{SrAl}_2\text{O}_4\text{:Dy}^{3+}$  phosphor is 5965 K, which is well under the acceptable ranged and can be considered "cool" in appearance.

### 3.11 Long afterglow (decay)

Figure 11 shows the typical decay curves of  $\text{SrAl}_2\text{O}_4\text{:Dy}^{3+}$  phosphor. The initial afterglow intensity of the sintered  $\text{SrAl}_2\text{O}_4\text{:Dy}^{3+}$  phosphor was high. The decay times of phosphor can be calculated by a curve fitting technique, and decay curves fitted by the sum of two exponential components have different decay times [42].

$$I = A_1 \exp(-t/\tau_1) + A_2 \exp(-t/\tau_2) \quad (6)$$

where,  $I$  is phosphorescence intensity,  $A_1$ ,  $A_2$  are constants,  $t$  is time,  $\tau_1$  and  $\tau_2$  are decay times (in millisecond) for the exponential components. Decay curves are successfully fitted by the Eq. (6) and the fitting curve result are shown in Table 2. The results indicated that the, afterglow decay curves are composed of two regimes, i.e., the initial rapid decaying process and the subsequent slow decaying process (Table 3).

$\text{Dy}^{3+}$  is an important rare earth ion in the development of phosphors with long lasting afterglow, playing a crucial role. The dopant  $\text{Dy}^{3+}$  is a famous trap creating ion, which can greatly prolong the afterglow. It is reasonable to consider that the role of doping  $\text{Dy}^{3+}$  ions is to introduce new types of traps or significantly increase the concentration of traps responsible for the afterglow. The afterglow intensity of the persistent phosphor depends on the densities of the traps electrons, while the duration of afterglow depends on the depth of the trapped electrons. The number of trapped charge carrier, in term, depends on the concentration of oxygen vacancies/ $\text{Dy}^{3+}$  and the trap depth of it. For a suitable trap depth, the trap concentration is directly depends on the dysprosium ions [43, 44].

### 3.12 Mechanoluminescence (ML)

Mechanoluminescence (ML) (also known as Triboluminescence) is an important physical phenomenon where an emission of light is observed due to mechanical deformation of materials when they are subjected to some mechanical stress like rubbing, cleavage, compressing, impulsive crushing, grinding, shaking etc. The ML phenomenon has been known for centuries; however, it is only in recent years that this phenomenon has attracted more attention because of its potential application for sensing structural damage, fractures, and deformation. In the ML studies, an impulsive deformation technique has been used for measurements [45].

### 3.13 Experimental setup for mechanoluminescence measurement

The experimental set up used for the impulsive deformation of ML was shown in Fig. 12. A load of particular mass and shape was dropped from different heights for striking the prepared  $\text{SrAl}_2\text{O}_4\text{:Dy}^{3+}$  phosphor at different impact velocities. In this experiment, the mass of the dropping load was 400 g and shape of the load was cylindrical. The phosphor under study was placed on the upper surface of a transparent lucite plate and it was then covered with a thin aluminum foil and fixed with adhesive tape. The foil reflects light and prevents scattering of the fragments during the impact of a moving piston onto the prepared phosphor. This arrangement eliminates the error in the ML measurement due to the scattering of the crystallite fragments during the impact of the load onto the phosphor. The housing is made up of thick soft iron to provide shielding from light and magnetic field. The slit arrangement at the window is provided to adjust the size of the window according to the incident beam. When the phosphor placed on the lucite plate was crushed by impact of the load, light is emitted [46].

**Fig. 11** Decay curves of SrAl<sub>2</sub>O<sub>4</sub>:Dy<sup>3+</sup> phosphor

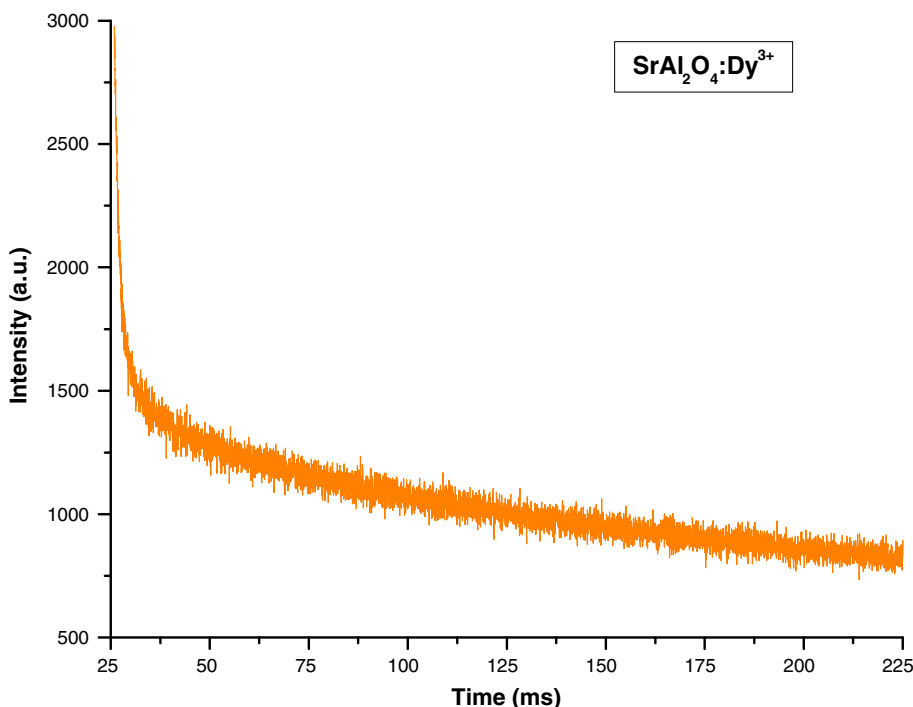


**Table 3** Fitting results of the decay curves

Phosphor	$\tau_1$ (ms)	$\tau_2$ (ms)
SrAl <sub>2</sub> O <sub>4</sub> :Dy <sup>3+</sup>	1.81	99.72

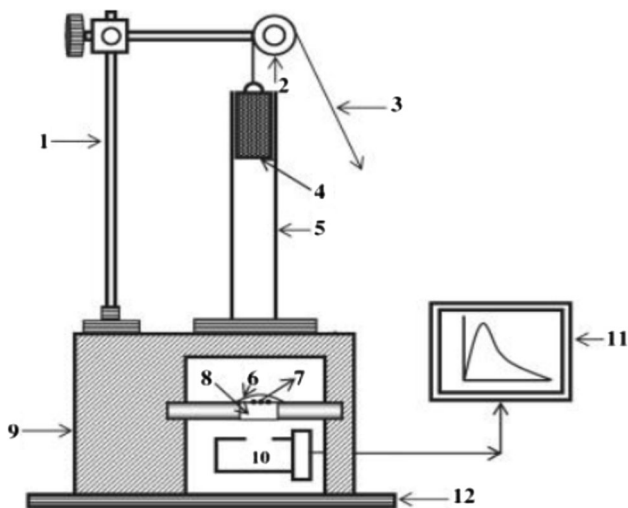


**Fig. 12** Schematic diagram of the experimental setup for ML measurement

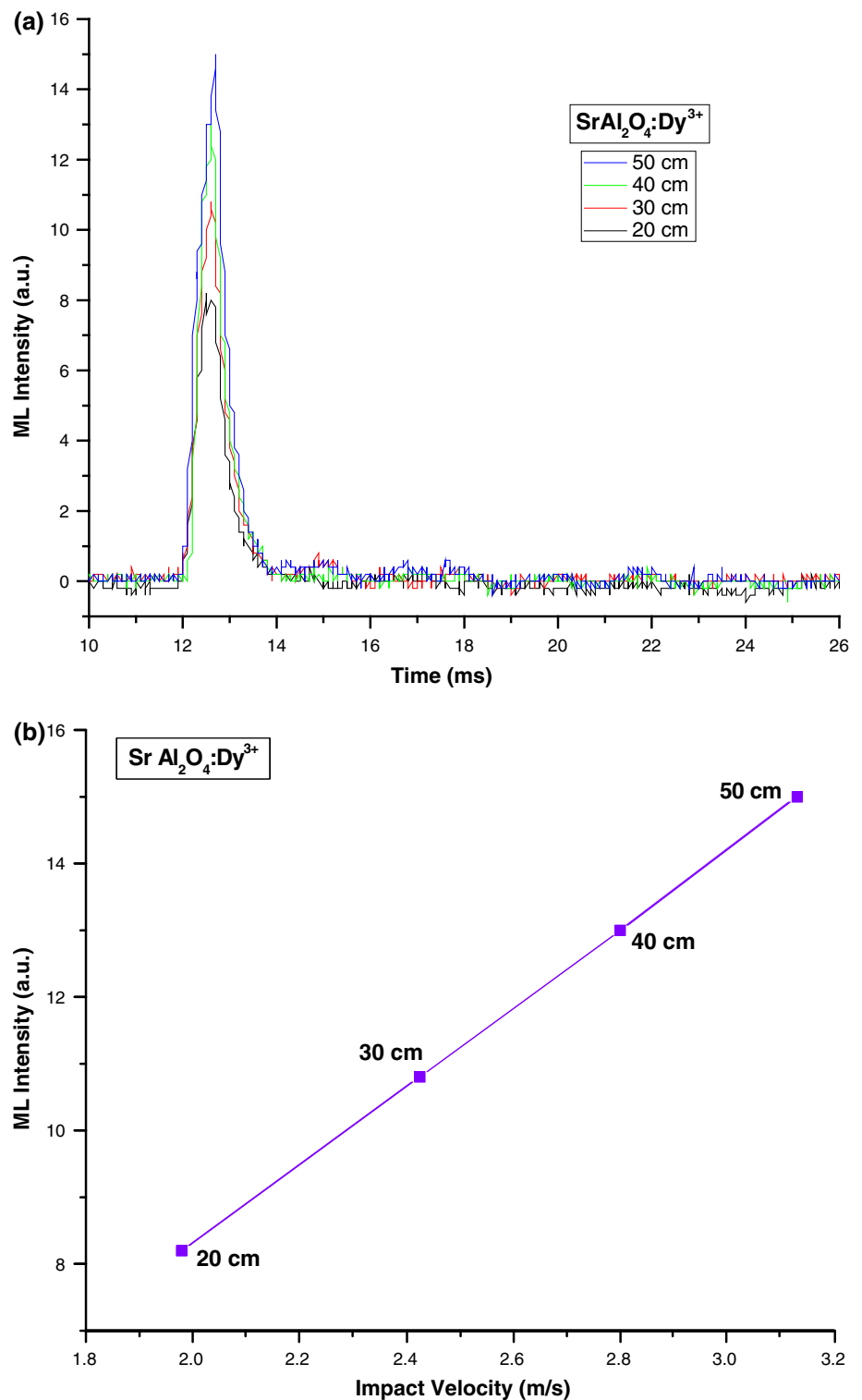
In the Fig. 12, 1—Stand; 2—Pulley; 3—Metallic wire; 4—Load; 5—Guiding cylinder; 6—Aluminium foil; 7—Phosphor; 8—Transparent Lucite plate; 9—Wooden block;

10—Photomultiplier tube (PMT); 11—Storage oscilloscope; 12—Iron base mounted on a table.

By changing the distance between the piston to be dropped and the sample placed on the lucite plate, the impact velocity ( $v_0$ ) of the load could be changed from 197 cm/s to 328 cm/s, since the pulley and the guiding cylinder used were of negligible friction, the impact velocity ( $v_0$ ) was taken as  $\sqrt{2gh}$ , where “g” is the acceleration due to gravity and “h” is the height through which the load is dropped freely. An RCA 931A photomultiplier tube (PMT) was placed below the transparent lucite plate. The PMT was run at 750 Volts. The output of PMT was connected to the phosphorescent screen oscilloscope (Scientific 300 MHz, SM 340). The ML glow curve can be plotted with the help of SM-340 application software installed in a computer attached with the storage oscilloscope [47].

Figure 13a shows that the characteristics curve between ML intensity versus time for different heights ( $h = 20, 30, 40, 50$  cm). The phosphor was fracture via dropping a load [moving piston] of particular mass (400 g) and cylindrical shape on the SrAl<sub>2</sub>O<sub>4</sub>:Dy<sup>3+</sup> phosphor. The velocity of the moving piston, holding the impact mass, could be changed, by changing the height through which it was dropped. Every time for the ML measurement, the quantity of SrAl<sub>2</sub>O<sub>4</sub>:Dy<sup>3+</sup> phosphor was kept constant (8 mg). When the moving piston is dropped onto the prepared phosphor at different height, light is emitted. The photon emission time is nearly 2 ms, when prepared SrAl<sub>2</sub>O<sub>4</sub>:Dy<sup>3+</sup> phosphor

**Fig. 13** **a** ML intensity versus time curve of  $\text{SrAl}_2\text{O}_4:\text{Dy}^{3+}$  phosphor. **b** ML intensity versus impact velocity curve of  $\text{SrAl}_2\text{O}_4:\text{Dy}^{3+}$  phosphor



fractures. In these ML measurements, maximum ML intensity has been obtained for the 50 cm dropping height and ML intensity increases linearly with the increases the falling height of the moving piston. The sintered

$\text{SrAl}_2\text{O}_4:\text{Dy}^{3+}$  phosphor was not irradiated by any excitation source [48].

Figure 13b shows the curve of ML intensity versus impact velocities for  $\text{SrAl}_2\text{O}_4:\text{Dy}^{3+}$  phosphor. It is seen



that, ML intensity increases linearly with increasing impact velocity [ $v_0 = \sqrt{2gh}$ , (where “g” is the acceleration due to gravity and “h” is the height through which the load is dropped freely)] of the moving piston. The ML intensity of  $\text{SrAl}_2\text{O}_4:\text{Dy}^{3+}$  phosphor increases linearly with increasing the mechanical stress.

The space group of  $\text{SrAl}_2\text{O}_4:\text{Dy}^{3+}$  phosphor is  $P2_1$ , which indicates that the crystal belongs to non-piezoelectric structure. When a mechanical stress, such as compress, friction, and striking and so on, was applied on the sintered  $\text{SrAl}_2\text{O}_4:\text{Dy}^{3+}$  phosphors, piezo-electric field can be produced. Therefore, in such phosphor the ML excitation may be caused by the local piezoelectric field near the impurities and defects in the crystals. During the impact on the material, one of its newly created surfaces gets positively charged and the other surface of the crack gets negatively charged [Fig. 14 Langevin model]. Thus, an intense electric field of the order of  $10^6\text{--}10^7$  Volt  $\text{cm}^{-1}$  is produced [49]. Under such order of piezoelectric field, the ejected electrons from the negatively charged surface may be accelerated and their impact on the positively charged surfaces of the cracks may excite the luminescence centers such as  $\text{Dy}^{3+}$  ions. Subsequently, the de-excitation of excited  $\text{Dy}^{3+}$  ions may give rise to the light emission due to the transition from  ${}^4\text{F}_{9/2}$  state to  ${}^6\text{H}_j$  state (where  $j = 15/2, 13/2, 11/2$ ) respectively, emitting radiation at 480, 573 and 670 nm. With the increase in impact velocity, more compression of the sample takes place, and therefore, more area of the newly created surface takes place. Thus, the ML intensity will increase with increasing value of the impact velocity [50].

Thus, depending on the prevailing conditions, recombination luminescence may be produced. For the impact velocity, the impact pressure  $P_0$  will be equals to,

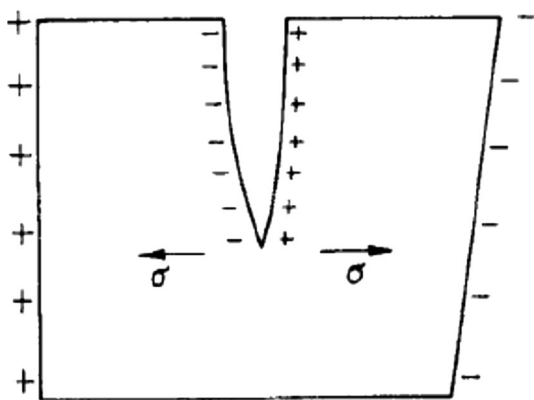


Fig. 14 Langevin model for the piezo-electrification induce phosphor

$P_0 = Zv_0$ , where  $Z$  is a constant. With increasing value impact velocity of the trap depth will decrease, therefore, the trap depth beyond a particular pressure the traps will be unstable and they will be de-trapped, in which the number of de-trapped electrons will increases with the increasing impact velocity. Thus, the ML intensity will increase proportionally with increasing value of impact velocity. As the impact velocity increases, the impact pressure also increases leading to the increase in the electric field at local region which causes the decrease in trap depth. Hence the probability of de-trapping increases. From Fig. 13b, it can be seen that with increasing impact velocity, ML intensity also increases linearly i.e., the ML intensity of  $\text{SrAl}_2\text{O}_4:\text{Dy}^{3+}$  phosphor are lineally proportional to the magnitude of the impact velocity [47, 48].

When the surface of an object was coated with the ML materials, the stress distribution in the object beneath the layer could be reflected by the ML brightness and could be observed. Based on the above analysis this phosphor can also be used as sensors to detect the stress of an object. Thus the present investigation indicates that the piezo-electrification is responsible to produce ML in prepared phosphor.

### 4 Conclusion

In summary,  $\text{SrAl}_2\text{O}_4:\text{Dy}^{3+}$  phosphor was prepared by the traditional combustion synthesis method. The monoclinic structure of prepared phosphor was confirmed by the XRD. From TL glow curve, initially TL intensity increase with increasing UV irradiation time and maximum for 20 min irradiation time. It is predicted that, with the increasing UV irradiation time, density of charge carrier may have been increasing, but after a specific irradiation time, charge carriers density decreases, results in decreasing the TL intensity. Under the ultra-violet (UV) excitation, the prepared  $\text{SrAl}_2\text{O}_4:\text{Dy}^{3+}$  phosphor would emit blue, yellow and red light with peak at 480 nm, 573 nm and 670 nm corresponds to the transitions of  ${}^4\text{F}_{9/2} \rightarrow {}^6\text{H}_{15/2}$ ,  ${}^4\text{F}_{9/2} \rightarrow {}^6\text{H}_{13/2}$  and  ${}^4\text{F}_{9/2} \rightarrow {}^6\text{H}_{11/2}$  respectively. The three emission bands of the  $\text{SrAl}_2\text{O}_4:\text{Dy}^{3+}$  phosphor combines to give out white light, which was confirmed from the calculated CIE coordinates which were found to be very close to standard white light for human eyes. CCT values calculated were found in the acceptable range and can be described as “cool” in appearance. It is worthy to note that the dependence between ML intensity of  $\text{SrAl}_2\text{O}_4:\text{Dy}^{3+}$  phosphor to the impact velocity is close to linearity, which suggests that these phosphors can be used as sensors to detect the stress of an object.

## References

- C. Zhao, D. Chen, Y. Yuan, M. Wu, Synthesis of  $\text{Sr}_4\text{Al}_{14}\text{O}_{25}:\text{Eu}^{2+}, \text{Dy}^{3+}$  phosphor nanometer powders by combustion processes and its optical properties. *Mater. Sci. Eng. B* **133**, 200–204 (2006)
- K.E. Foka, F.B. Dejene, H.C. Swart, Photoluminescence properties of  $\text{Ce}^{3+}$  doped  $\text{SrAl}_2\text{O}_4$  prepared using the solution combustion method. *Phys. B* **439**, 177–180 (2014)
- B.M. Mothudi, O.M. Ntwaeaborwa, J.R. Botha, H.C. Swart, Photoluminescence and phosphorescence properties of  $\text{MAl}_2\text{O}_4:\text{Eu}^{2+}, \text{Dy}^{3+}$  ( $\text{M} = \text{Ca}, \text{Ba}, \text{Sr}$ ) phosphors prepared at an initiating combustion temperature of 500 °C. *Phys. B* **404**, 4440–4444 (2009)
- F. Clabau, X. Rocquefelte, S. Jobic, P. Deniard, M.H. Whangbo, A. Garcia, T. Le Mercier, On the phosphorescence mechanism in  $\text{SrAl}_2\text{O}_4:\text{Eu}^{2+}$  and its codoped derivatives. *Solid State Sci.* **9**, 608–612 (2007)
- E. Nakazawa, Y. Murazaki, S. Saito, Mechanism of the persistent phosphorescence in  $\text{Sr}_4\text{Al}_{14}\text{O}_{25}:\text{Eu}$  and  $\text{Sr}_4\text{Al}_{14}\text{O}_{25}:\text{Eu}$  codoped with rare earth ions. *J. Appl. Phys.* **100**, 113–118 (2006)
- R. Chen, Y. Wang, Y. Hu, Z. Hu, C. Liu, Modification on luminescent properties of  $\text{SrAl}_2\text{O}_4:\text{Eu}^{2+}, \text{Dy}^{3+}$  phosphor by  $\text{Yb}^{3+}$  ions doping. *J. Lumin.* **128**, 1180–1184 (2008)
- Z. Tang, F. Zhang, Z. Zhang, C. Huang, Y. Lin, Luminescent properties of  $\text{SrAl}_2\text{O}_4:\text{Eu}, \text{Dy}$  material prepared by the gel method. *J. Eur. Ceram. Soc.* **20**, 2129–2132 (2000)
- O. Arellano-Tánori, R. Meléndrez, M. Pedroza-Montero, B. Castañeda, V. Chernov, W.M. Yen, M. Barboza-Flores, Persistent luminescence dosimetric properties of UV-irradiated  $\text{SrAl}_2\text{O}_4:\text{Eu}^{2+}, \text{Dy}^{3+}$  phosphor. *J. Lumin.* **128**, 173–184 (2008)
- H.B. Yuan, W. Jia, S.A. Basun, L. Lu, R.S. Meltzer, W.M. Yen, The long-persistent photoconductivity of  $\text{SrAl}_2\text{O}_4:\text{Eu}^{2+}, \text{Dy}^{3+}$  single crystals. *J. Electrochem. Soc.* **147**, 3154–3156 (2000)
- T. Peng, H. Yang, X. Pu, B. Hu, Z. Jiang, C. Yan, Combustion synthesis and photoluminescence of  $\text{SrAl}_2\text{O}_4:\text{Eu}, \text{Dy}$  phosphor nanoparticles. *Mater. Lett.* **58**, 352–356 (2004)
- Z. Fu, L. Ma, S. Sahi, R. Hall, W. Chen, Influence of doping concentration on valence states of europium in  $\text{SrAl}_2\text{O}_4:\text{Eu}$  phosphors. *J. Lumin.* **143**, 657–662 (2013)
- D.S. Kshatri, A. Khare, P. Jha, Effects of Dy concentration on luminescent properties of  $\text{SrAl}_2\text{O}_4:\text{Eu}$  phosphors. *Optik* **124**, 2974–2978 (2013)
- S.K. Sharma, S.S. Pitale, M.M. Malik, T.K. GunduRao, S. Chawla, M.S. Qureshi, R.N. Dubey, Spectral and defect analysis of Cu-doped combustion synthesized new  $\text{SrAl}_4\text{O}_7$  phosphor. *J. Lumin.* **130**, 240–245 (2010)
- B.M. Smets, Phosphors based on rare-earths, a new era in fluorescent lighting. *Mater. Chem. Phys.* **16**(3–4), 283–288 (1987)
- C.R. Ronda, Recent achievements in research on phosphors for lamps and displays. *J. Lumin.* **49**, 72–79 (1997)
- G. Ju, Y. Hu, L. Chen, X. Wang, Z. Mu, Concentration quenching of persistent luminescence. *Phys. B* **415**, 1–4 (2013)
- Y. Cheng, Y. Zhao, Y. Zhang, X. Cao, Preparation of  $\text{SrAl}_2\text{O}_4:\text{Eu}^{2+}, \text{Dy}^{3+}$  fibers by electrospinning combined with sol–gel process. *J. Colloid Interface Sci.* **344**, 321–326 (2010)
- N. Dubnikova, E. Garskaite, A. Beganskiene, A. Kareiva, Sol–gel synthesis and characterization of sub-microsized lanthanide (Ho, Tm, Yb, Lu) aluminium garnets. *Opt. Mater.* **33**, 1179–1184 (2011)
- B. Schrader, *Infrared and Raman spectroscopy: methods and applications* (VCH, Weinheim, 1995)
- K. Nakamoto, *Infrared and Raman spectra of inorganic and coordination compounds* (Wiley, New York, 1986)
- Y. Karabulut, A. Canimoglu, Z. Kotan, O. Akyuz, E. Ekdal, Luminescence of dysprosium doped strontium aluminate phosphors by codoping with manganese ion. *J. Alloy. Compd.* **583**, 91–95 (2014)
- M. Ayvacıklı, A. Ege, N. Can, Radioluminescence of  $\text{SrAl}_2\text{O}_4:\text{Ln}^{3+}$  ( $\text{Ln} = \text{Eu}, \text{Sm}, \text{Dy}$ ) phosphor ceramic. *Opt. Mater.* **34**, 138–142 (2011)
- P.T. Ji, X.Y. Chen, Y.Q. Wu, Encapsulating  $\text{MAl}_2\text{O}_4:\text{Eu}^{2+}, \text{Dy}^{3+}$  ( $\text{M} = \text{Sr}, \text{Ca}, \text{Ba}$ ) phosphors with triethanolamine to enhance water resistance. *Appl. Surf. Sci.* **258**, 1888–1893 (2011)
- M. Misevicius, O. Scit, I. Grigoraviciute-Puroniene, G. Degutis, I. Bogdanoviciene, A. Kareiva, Sol–gel synthesis and investigation of un-doped and Ce-doped strontium aluminates. *Ceram. Int.* **38**, 5915–5924 (2012)
- A. Nag, T.R.N. Kutty, The mechanism of long phosphorescence of  $\text{SrAl}_{2-x}\text{B}_x\text{O}_4$  ( $0 < x < 0.2$ ) and  $\text{Sr}_4\text{Al}_{14-x}\text{B}_x\text{O}_{25}$  ( $0.1 < x < 0.4$ ) codoped with  $\text{Eu}^{2+}$  and  $\text{Dy}^{3+}$ . *Mater. Res. Bull.* **39**, 331–342 (2004)
- T. Katsumata, R. Sakai, S. Komuro, T. Morikawa, Thermally stimulated and photostimulated luminescence from long duration phosphorescent  $\text{SrAl}_2\text{O}_4:\text{Eu}, \text{Dy}$  crystals. *J. Electrochem. Soc.* **150**(5), 111–114 (2003)
- M. Mashangva, M.N. Singh, T.B. Singh, Estimation of optical trapping relevant to persistence luminescence Indian. *J. Pure Appl. Phys.* **49**, 583–589 (2011)
- I.P. Sahu, D.P. Bisen, N. Brahme, Dysprosium doped di-strontium magnesium di-silicate white light emitting phosphor by solid state reaction method. *Displays* **35**, 279–286 (2014)
- I.P. Sahu, D.P. Bisen, N. Brahme, Structural characterization and optical properties of dysprosium doped strontium calcium magnesium di-silicate phosphor by solid state reaction method. *Displays* **38**, 68–76 (2015)
- F.M. Emen, N. Kulcu, A.N. Yazici, Synthesis, characterization and luminescence properties of the long afterglow Phosphor  $\text{Ba}_4\text{Al}_{14}\text{O}_{25}:\text{Eu}, \text{Dy}$ . *Eur J Chem* **1**(1), 28–32 (2010)
- Z. Yuan, C. Chang, D. Mao, W. Ying, Effect of composition on the luminescent properties of  $\text{Sr}_4\text{Al}_{14}\text{O}_{25}:\text{Eu}^{2+}, \text{Dy}^{3+}$  phosphors. *J. Alloys Compd.* **377**(1–2), 268–271 (2004)
- F.M. Emen, V.E. Kafadar, N. Kulcu, A.N. Yazici, Thermoluminescence studies and detailed kinetic analysis of  $\text{Sr}_4\text{Al}_{14}\text{O}_{25}:\text{Eu}^{2+}, \text{Dy}^{3+}$  phosphor. *J. Lumin.* **144**, 133–138 (2013)
- V. Pagonis, G. Kitis, C. Furetta, *Numerical and practical exercises in thermoluminescence* (Springer, Berlin, 2006)
- R. Chen, S.W.S. McKeever, *Theory of thermoluminescence and related phenomena* (World Scientific Publications, London, NJ, Singapore, 1997), p. 576
- J. Kuang, Y. Liu, J. Zhang, White-light-emitting long-lasting phosphorescence in  $\text{Dy}^{3+}$  doped  $\text{SrSiO}_3$ . *J. Solid State Chem.* **179**, 266–269 (2006)
- Rama Raju GS, Park JY, Jung HC, Moon BK, Jeong JH, Kim JH, Blue and green emissions with high color purity from nanocrystalline  $\text{Ca}_2\text{Gd}_8\text{Si}_6\text{O}_{26}:\text{Ln}$  ( $\text{Ln} = \text{Tm}$  or  $\text{Er}$ ) phosphors. *Curr. Appl. Phys.* **9**, 92–97 (2009)
- Y. Chen, X. Cheng, M. Liu, Z. Qi, C. Shi, Comparison study of the luminescent properties of the white-light long afterglow phosphors:  $\text{Ca}_x\text{MgSi}_2\text{O}_{5+x}:\text{Dy}^{3+}$ . *J. Lumin.* **129**, 531–535 (2009)
- A. Zukauskas, M.S. Shur, R. Gaska, *Introduction to solid state lighting* (Wiley, New York, 2002)
- I.P. Sahu, Luminescence properties of dysprosium doped calcium magnesium silicate phosphor by solid state reaction method. *J. Alloys Compd.* (2015). doi:10.1016/j.jallcom.2015.06.011
- CIE (1931) International Commission on Illumination. Publication CIE No. 15 (E-1.3.1)
- C.S. McCamy, Correlated color temperature as an explicit function of chromaticity coordinates. *Color Res. Appl.* **17**, 142–144 (1992)
- R. Shrivastava, J. Kaur, Studies on long lasting optical properties of  $\text{Eu}^{2+}$  and  $\text{Dy}^{3+}$  doped di-barium magnesium silicate phosphors. *Chin. Chem. Lett.* (2015). doi:10.1016/j.ccllet.2015.05.028

43. T. Aitasalo, J. Holsa, H. Jungner, M. Lastusaari, J. Niittykoski, Thermoluminescence study of persistent luminescence materials:  $\text{Eu}^{2+}$  and  $\text{R}^{3+}$  doped calcium aluminates,  $\text{CaAl}_2\text{O}_4:\text{Eu}^{2+}$ ,  $\text{R}^{3+}$ . *J. Phys. Chem. B* **110**, 4589–4598 (2006)
44. I.P. Sahu, The role of europium and dysprosium in the bluish-green long lasting  $\text{Sr}_2\text{Al}_2\text{SiO}_7:\text{Eu}^{2+}$ ,  $\text{Dy}^{3+}$  phosphor by solid state reaction method. *J. Mater. Sci. Mater. Electron.* (2015). doi:[10.1007/s10854-015-3327-2](https://doi.org/10.1007/s10854-015-3327-2)
45. D.R. Vij, *Luminescence of solids* (Plenum Press, New York, 1998)
46. B.P. Chandra, Development of mechanoluminescence technique for impact studies. *J. Lumin.* **131**, 1203–1210 (2011)
47. I.P. Sahu, D.P. Bisen, N. Brahme, L. Wanjari, R.K. Tamrakar, Structural Characterization and luminescence properties of bluish-green emitting  $\text{SrCaMgSi}_2\text{O}_7:\text{Eu}^{2+}$ ,  $\text{Dy}^{3+}$  phosphor by solid state reaction method. *Res. Chem. Intermed.* (2015). doi:[10.1007/s11164-015-1929-1](https://doi.org/10.1007/s11164-015-1929-1)
48. I.P. Sahu, D.P. Bisen, N. Brahme, Luminescence properties of  $\text{Eu}^{2+}$  and  $\text{Dy}^{3+}$  doped  $\text{Sr}_2\text{MgSi}_2\text{O}_7$  and  $\text{Ca}_2\text{MgSi}_2\text{O}_7$  phosphors by solid state reaction method. *Res. Chem. Intermed.* (2014). doi:[10.1007/s11164-014-1767-6](https://doi.org/10.1007/s11164-014-1767-6)
49. B.P. Chandra, A.S. Rathore, Classification of mechanoluminescence. *Cryst. Res. Technol.* **30**, 885–896 (1995)
50. I.P. Sahu, D.P. Bisen, N. Brahme, Luminescence properties of green emitting  $\text{Ca}_2\text{MgSi}_2\text{O}_7:\text{Eu}^{2+}$  phosphor by solid state reaction method. *Lumin J Biol Chem Lumin* (2015). doi:[10.1002/bio.2869](https://doi.org/10.1002/bio.2869)